Lab on a Chip

PAPER

View Article Online
View Journal | View Issue

Cite this: *Lab Chip*, 2016, **16**, 4560

An inkjet printed, roll-coated digital microfluidic device for inexpensive, miniaturized diagnostic assays†

Christopher Dixon,[a] Alphonsus H. C. Ng,‡[bc] Ryan Fobel,[bc] Mark B. Miltenburg[a] and Aaron R. Wheeler*[abc]

Received 24th August 2016,
Accepted 21st October 2016

DOI: 10.1039/c6lc01064d

www.rsc.org/loc

The diagnosis of infectious disease is typically carried out at the point-of-care (POC) using the lateral flow assay (LFA). While cost-effective and portable, LFAs often lack the clinical sensitivity and specificity required for accurate diagnoses. In response to this challenge, we introduce a new digital microfluidic (DMF) platform fabricated using a custom inkjet printing and roll-coating process that is scalable to mass production. The performance of the new devices is on par with that of traditional DMF devices fabricated in a cleanroom, with a materials cost for the new devices of only US $0.63 per device. To evaluate the usefulness of the new platform, we performed a 13-step rubella virus (RV) IgG immunoassay on the inkjet printed, roll-coated devices, which yielded a limit of detection of 0.02 IU mL^{-1}, well below the diagnostic cut-off of 10 IU mL^{-1} for RV infection and immunity. We propose that this represents a breakthrough for DMF, lowering the costs to a level such that the new platforms will be an attractive alternative to LFAs for the diagnosis of infectious disease at the POC.

Introduction

Infectious diseases are typically diagnosed in centralized laboratories. This is unfortunate, as such tests are expensive[1] (putting them out of reach of some communities) and slow[2] (which can have life-or-death implications). There is currently great enthusiasm for the development of inexpensive tests that can be implemented at the "point of care" (POC) to allow for rapid diagnosis of infectious diseases.[3,4] The mechanism envisioned for most such POC tests is the lateral flow assay (LFA), a technique in which fluid is transported (or "wicked") through absorptive media by capillary action. LFAs have been used for portable tests for decades (*e.g.*, over-the-counter pregnancy tests), and the lab-on-a-chip community has recently combined LFAs with clever patterning techniques to form a device format known as "paper microfluidics."[5] There is great interest in using paper microfluidics/LFAs for portable applications because of very low device cost,[6] the stability of dried reagents,[7] and the reduced dependence on expensive analytical instrumentation.[8] The use of LFAs solves both problems mentioned above (expense and portability), but brings a new challenge – many LFAs lack the clinical sensitivity and specificity needed to facilitate unambiguous diagnoses.[9] Centralized laboratory tests (which have high clinical sensitivity and specificity) typically require complex multi-step assays with iterative buffer exchanges and washing steps to suppress background and enhance signal; these steps are often impossible in the LFA format. These challenges have been partly addressed by three-dimensional channel networks,[10] length-programmed reagent delivery,[11] cut-out fluidic switches,[12] and clever folding tricks;[13] however, these techniques require operator intervention which introduces other undesirable complications.

An alternative to LFAs and paper microfluidics is digital microfluidics (DMF).[14] DMF is a robust liquid handling technology that comprises the manipulation of discrete picolitre to microlitre-sized liquid droplets using electrostatic forces. In the two-plate DMF format, droplets are sandwiched between a counter-electrode top plate and a bottom plate bearing an array of insulated driving electrodes. In this configuration, individual droplets, each serving as micro-reactors, can be dispensed, mixed, merged, and separated, making DMF a powerful sample handling and chemical processing technique. Complex multi-step operations (*e.g.*, washing,[15] solvent exchanges,[16] and extractions[17]) can be performed in an

[a] *Department of Chemistry, University of Toronto, 80 St. George Street, Toronto, Ontario, M5S 3H6, Canada. E-mail: aaron.wheeler@utoronto.ca; Fax: +1 416 946 3865; Tel: +1 416 946 3864*
[b] *Donnelly Centre for Cellular and Biomolecular Research, University of Toronto, 160 College Street, Toronto, Ontario, M5S 3H6, Canada*
[c] *Institute for Biomaterials and Biomedical Engineering, University of Toronto, 164 College Street, Toronto, Ontario, M5S 3H6, Canada*
† Electronic supplementary information (ESI) available. See DOI: 10.1039/c6lc01064d
‡ Current address: Division of Chemistry and Chemical Engineering, California Institute of Technology, 1200 E. California Boulevard, Pasadena, California, 91125, USA

automated fashion, and since droplets are individually addressable on a generic device geometry, experiments can be reconfigured on-the-fly. These properties (and others) are making DMF an increasingly popular tool for miniaturizing applications ranging from chemical synthesis,[18–21] to chemical analysis,[22–25] and cell culture.[26–29]

While DMF has proven to be a useful technology, one of its leading challenges is fabrication – devices are typically manufactured on glass substrates with slow and expensive photolithography, wet-etching, vapour deposition, and spin-coating techniques (often requiring a clean room facility).[16] There have been various efforts at forming DMF devices using cleanroom-free methods over the years,[30–33] but the performance of devices generated using these techniques was limited, and the techniques themselves were typically not scalable for mass manufacturing. In a critical breakthrough, two groups recently reported methods for forming devices by inkjet printing[34,35] (IJP). These techniques are inexpensive (printing devices onto paper), the device performances are outstanding, and the manufacturing processes have the potential for scaling up to high-volume manufacturing. This is an exciting advance, but the two previous reports leave much to be desired – one[34] has only been demonstrated for one-plate devices (which have limited functionality – likely not useful for high-performance diagnostic assays), while the other[35] uses the powerful two-plate format (which is well-suited for high-performance diagnostic assays[36]), but (a) requires an expensive industrial-grade printer, and (b) the device top plates were formed from conventional, expensive materials used in the cleanroom (indium-tin oxide-coated glass). But the biggest drawback for both of the IJP methods reported previously[34,35] is that the dielectric and hydrophobic layers were applied using cleanroom-techniques (*i.e.*, spin-coating and chemical vapour deposition) that are not compatible with a scalable, inexpensive production scheme. These drawbacks must be overcome for IJP-DMF devices to compete with the very low cost of LFAs.

Here we present the next chapter in inkjet printed DMF device fabrication. In this technique, which features the powerful two-plate device format, DMF driving electrodes are formed using an inexpensive consumer-grade inkjet printer, and the dielectric and hydrophobic layers were applied (for the first time) using a method that is directly scalable to the powerful technique of roll-to-roll fabrication (useful for forming inexpensive, disposable microfluidic devices[37]) for mass production. The new devices were demonstrated to be useful for implementing complex, multi-step diagnostic assays, which leads us to propose that the techniques introduced here represent an attractive alternative to LFAs for implementation of POC diagnostics for infectious disease.

Materials and methods

Reagents and materials

Unless otherwise specified, reagents were purchased from Sigma Aldrich (Oakville, ON). Deionized (DI) water had a resistivity of 18 MΩ cm at 25 °C. Tetronic 90R4 (BASF Corp., Germany) was generously donated by Brenntag Canada (Toronto, ON). Novele IJ-220 inkjet printing media and Metalon JS-B25P silver nanoparticle ink were purchased from NovaCentrix (Austin, TX). Empty ink cartridges (black – ARC-T0601-EC; cyan – ARC-T0602-EC; magenta – ARC-T0603-EC; and yellow – ARC-T0602-EC) were purchased from MIS Associates, Inc. (Auburn Hills, MI). Glass slides were purchased from S.I. Howard Glass Co., Inc. (Worcester, MA). ITO-PET substrates were purchased from Sigma Aldrich (Oakville, ON) and ITO-Glass substrates were purchased from Delta Technologies Ltd. (Stillwater, MN). Cyanoresin CR-S cyanoethyl pullulan (CEP) was purchased from Shin-Etsu Chemical Co., Ltd. (Tokyo, Japan). FluoroPel PFC 1101V was purchased from Cytonix, LLC (Beltsville, MD). Immunoassay reagents were adapted from the Architect rubella IgG assay kit from Abbott Laboratories (Abbott Park, IL), including RV IgG calibrators and virus-coated paramagnetic particles. Superblock Tris-buffered saline, SuperSignal ELISA Femto chemiluminescent substrate comprising stable hydrogen peroxide (H_2O_2) and luminol-enhancer solution were purchased from Thermo Fischer Scientific (Rockford, IL). Custom digital microfluidic compatible wash buffer comprised Dulbecco's Phosphate Buffered Saline (DPBS) supplemented with Tetronic 90R4 (0.1% v/v). Conjugate working solutions and microparticle working suspension was prepared as described previously.[36]

DMF device fabrication and assembly

DMF bottom plates bearing patterns of driving electrodes were formed by inkjet printing and roll-coating (IJP-RC) on flexible substrates or by photolithography and etching, vapour deposition, and spin-coating (PLE-VD-SC) on glass substrates. For both, the design featured 8 reservoir electrodes (10.0 mm × 6.7 mm), 8 dispensing electrodes (5.2 mm × 2.4 mm) and 52 driving electrodes (each roughly 2.8 mm × 2.8 mm square, with an interdigitated off-set). In the IJP-RC design, the gaps between adjacent electrodes, as well as the widths of the traces connecting electrodes to contact pads, were both programmed to be 100 μm; the PLE-VD-SC design featured gaps and traces of 55 μm and 150 μm, respectively. The IJP-RC substrates were formed by printing electrode patterns onto a 1 m roll of inkjet printing media using an Epson C88+ inkjet printer (Seiko Epson Corporation, Tokyo, Japan). The default Gimp-Print driver (gimp-print.sourceforge.net) settings were used except for the following: paper type – premium glossy photo paper; image resolution – 2880 × 1440 DPI; print quality – best; shrink page – crop (preserve dimensions); printing direction – unidirectional; and image type – line art. After printing, the roll was allowed to dry at room temperature overnight, and then was coated with a ~16 μm-thick layer of CEP (from a 20% wt/wt solution in *N*,*N*-dimethylformamide) using a Mini Roll Coater (MRC) (FOM Technologies, Lyngby, Denmark). Optimum CEP coating parameters were as follows: flow rate – 2.0 mL min^{-1}; drum speed – 0.33 m min^{-1}; and drum temperature – 50 °C (other

parameters were also evaluated, and coating thicknesses were probed using contact profilometry). The roll was then coated with a ~0.38 μm-thick layer of FluoroPel PFC 1101V (from solution as received from the manufacturer) on the MRC, with coating parameters: flow rate – 1.0 mL min^{-1}; drum speed – 0.67 m min^{-1}; and drum temperature – 50 °C. After coating, the roll was diced into individual bottom plates with scissors, which were affixed to 50 mm × 75 mm glass slides with adhesive transfer tape F9460PC (3M Company, Maplewood, MN). Finally, the IJP-RC bottom plates were post-baked in an oven at 200 °C for two hours. The latter type of bottom plates (PLE-VD-SC substrates on glass) were formed using methods described previously.[16] Briefly, after patterning the electrodes, the electrode contacts were protected with dicing tape and then coated with a ~6.5 μm-thick layer of Parylene-C in a vapour deposition instrument (Specialty Coating Systems, Indianapolis, IN). The substrates were then coated with a ~70 nm-layer of FluoroPel PFC 1101V by spin-coating at 1500 rpm for 30 s. After removal of the dicing tape, the substrates were post-baked on a hot plate at 120 °C for 10 min.

DMF top plates were formed from two kinds of substrates – ITO-glass and ITO-PET. ITO-PET substrates were coated with FluoroPel PFC 1101V using the roll-coating (RC) process described above, and then were post-baked in an oven at 110 °C for 15 min. Substrates were diced into 25 mm × 75 mm pieces and affixed to glass slides with adhesive tape (as above). ITO-glass substrates were coated with FluoroPel PFC 1101V by spin-coating (SC) and then post-baked as described above. Two different types of fully assembled devices were formed, comprising fully roll-coated devices (*i.e.*, IJP-RC bottom plates with RC top plates, or "IJP-RC/RC"), and traditional devices (*i.e.*, PLE-VD-SC bottom plates with SC top plates, or "PLE-VD-SC/SC"). Each device was assembled by joining a top and bottom plate with two pieces of double-sided tape, resulting in an inter-plate gap of 180 μm. Unit droplets (*i.e.*, droplets covering a single driving electrode) on these devices had a volume of 1.20 μL.

Surface characterization

Scanning electron microscope (SEM) images were acquired with a Quanta FEG 250 SEM (FEI, Hillsboro, OR) in secondary electron mode with an accelerating voltage of 5 kV. Atomic force microscope (AFM) imaging was carried out with a Dimension Icon AFM (Bruker Corporation, Billerica, MA) in tapping mode. Profilometer measurements were made with an Alpha-Step 200 (KLA-Tencor, Milpitas, CA) with the scan length set at 400 μm, scan time at 8 s, and sample spacing at 1 μm.

Device operation

Devices were interfaced through pogo-pin connectors to one of two variations of the open-source DropBot controller, either with[15,36] or without[38] an integrated magnet and PMT. On both units, electrodes were switched using solid-state relays and velocities were measured using the open-source DropBot[38] impedance-based feedback circuit. Droplets were actuated by applying a force of ~20 μN mm^{-1} (75 V_{RMS} and 85 V_{RMS} for IJP-RC/RC and PLE-VD-SC/SC devices respectively) in a preprogrammed sequence.

Droplet velocity comparison

Unit droplets of immunoassay wash buffer were actuated back-and-forth between adjacent electrodes. In each experiment, the electrostatic driving force applied to the droplet was increased in 5 μN mm^{-1} steps (being careful to avoid applying forces high-enough to cause saturation effects[39]) and at each step, the resulting velocity was measured by DropBot.[38] At least 3 droplets were evaluated on separate devices for each condition evaluated. A movie illustrating one such test is included in the online ESI.†

Heterogeneous RV IgG ELISA

Heterogeneous RV IgG ELISAs were implemented in 13 steps on IJP-RC/RC devices. (1) A double-unit droplet of virus-coated paramagnetic particles (2.4 μL) was dispensed from a reservoir, the particles were immobilized, and the supernatant removed to waste using a stepper motor controlled magnet.[15,36] (2) A double-unit droplet of sample (2.4 μL, containing RV IgG calibrator at various concentrations in 4% BSA supplemented with 0.1% v/v Tetronic 90R4) was dispensed and delivered to the paramagnetic particles, actively mixed for 5 minutes, and then the supernatant was removed to waste. (3) A double-unit droplet of wash buffer (2.4 μL) was dispensed and delivered to the paramagnetic particles, actively mixed for 10 seconds, and then the supernatant was removed to waste. (4–6) Step 3 was repeated 3×. (7) A double-unit droplet of HRP conjugate solution (2.4 μL, containing HRP-conjugated antihuman IgG) was dispensed, delivered to the particles, and actively mixed for 5 minutes. (8–11) Step 3 was repeated 4×. (12) One unit droplet each of H_2O_2 and luminol-enhancer solutions (1.2 μL ea.) were dispensed, delivered to the particles, and actively mixed for 2 minutes. (13) The particle-substrate mixture was driven to the detection zone where the chemiluminescence was measured and averaged over 10 seconds using the integrated H10682-110 PMT (Hamamatsu Photonics K.K., Hamamatsu, Japan).

In each experiment, two 13-step assays were performed in parallel. Each assay was repeated three times for each concentration of IgG sample (0, 5, 15, 75 IU mL^{-1}). The data were plotted as a function of concentration and fit by least squares to a four parameter logistic nonlinear regression model. The limits of detection (LOD) and quantification (LOQ) were calculated as the concentrations (according to the fitted function) corresponding to the mean signal generated from blank measurements plus 3 (LOD) or 10 (LOQ) times the standard deviation of the blank measurements.

In wash-step experiments, the procedure was repeated with the original 13-steps (8 washes), the original procedure excluding steps 5–6 & 10–11 (4 washes), the original

procedure excluding steps 4–6 & 9–11 (2 washes), or the original procedure excluding steps 3–6 & 8–11 (0 washes). Three replicates were measured for each condition, applied to the 0 and 5 IU mL^{-1} RV IgG solutions, with data presented as the ratio of signal (5 IU mL^{-1}) to background (0 IU mL^{-1}).

Results and discussion

Inkjet printed DMF bottom plates

There is currently great enthusiasm for two recent reports[34,35] of inexpensive, inkjet printing-based methods to form digital microfluidic devices. These methods may eventually lead to DMF-based methods that can compete with LFAs for cost, but with the potential for improved diagnostic performance. As noted in the introduction, the methods reported previously[34,35] focused only on the formation of the electrodes (with little attention paid to the other materials required to fabricate devices); here, we introduce a complete solution for the fabrication of inexpensive DMF devices that are capable of performing the full suite of operations.

The first stage in developing the method described here was selection of a printer, printing media, and ink to generate a pattern of DMF driving electrodes, reservoirs, and contact pads on device bottom plates (Fig. 1a). Several options for each element (printer, medium, and ink) were evaluated on the basis of electrode pattern fidelity, spatial resolution, ink height and smoothness, printing speed, and cost. We ultimately chose an Epson C88+ inkjet printer (~US $100), a Novele IJ-220 printing medium (US $7.90 per m^2) and a silver colloid-based Metalon JS-B25P ink (US $5.00 per mL). In practice, the Novele substrate (~140 μm thick), which comprises a flexible, transparent PET-film coated with a ~35 μm-thick porous coating, was particularly useful because it can be loaded and printed in rolls (Fig. 1b); as far as we are aware, this is the first report of a "roll-based" method for fabricating DMF devices. Custom print-driver settings were developed and optimized to allow for printing with ink densities high enough for consistent generation of contiguous electrodes and traces with no breaks, while also maintaining a print resolution that ensured electrode gaps were without shorts. Ink traces formed using these settings (as catalogued in the methods section) were found to be conductive with no requirement of an annealing step, making the process remarkably straightforward to implement in or out of the laboratory.

A DMF bottom plate formed using the new methods is shown in Fig. 2a. As reported previously,[34,35] the critical characteristics for an IJP-DMF device are (i) pattern fidelity and spatial resolution, and (ii) ink height and roughness. For the former characteristic (i), contact profilometry was used to evaluate gaps between adjacent driving electrodes (Fig. 2b) and the electrode "traces" that connect driving electrodes to contact pads (Fig. 2c). Taking advantage of the differing interfacial energies of the ink, printing media, and air, electrode gaps were designed to be larger than desired, allowing for spreading of the ink on the printing media to reduce the gaps to a desired size. After optimization of the printing process, the gaps observed on the devices were ~50% smaller (avg. ±1 std. dev.: 55 ± 8 μm) and the traces were ~150% larger (avg. ±1 std. dev.: 148 ± 11 μm) than designed (100 μm for both).[40] Formation of devices with this gap- and trace-size was robust (*i.e.*, after optimization, unwanted shorts between electrodes or cuts to traces were not observed in many batches representing hundreds of devices printed), and thus these conditions were used for all of the devices described here. For the second characteristic (ii), profilometry revealed the ink to be ~1 μm thick (Fig. 2b and c). Surface roughness of the silver-ink electrodes was probed by scanning electron microscopy (SEM) (Fig. 2d) and atomic force microscopy (AFM) (Fig. 2e). As shown, the underlying silver ink layer appears to be porous but contiguous, with an irregular coating of ~250 nm dia. particles. We speculate that the particles, which were not observed to affect device performance, are silver-salt precipitates that form during the ink-drying process. The root-mean-square roughness

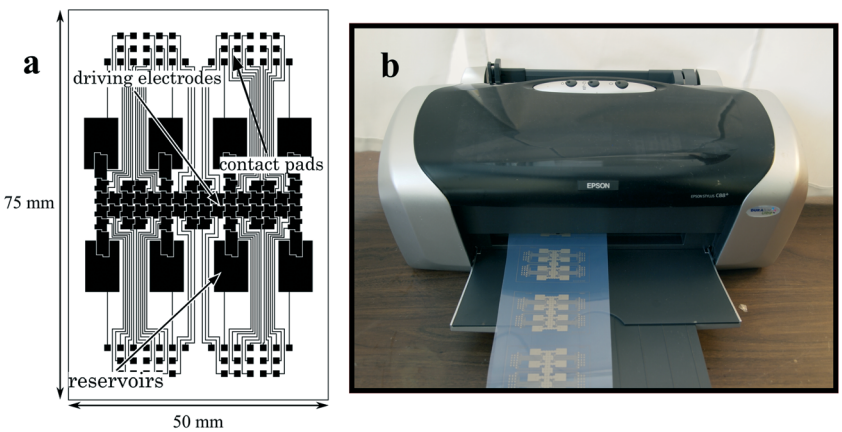

Fig. 1 Inkjet printed electrodes for digital microfluidics. (a) Top-view schematic of a substrate with interdigitated driving electrode array, reservoir electrodes, and contact pads for interfacing with the control system. (b) Picture of bottom-plates being printed onto a roll of Novele IJ-220 media using an Epson C88+ printer.

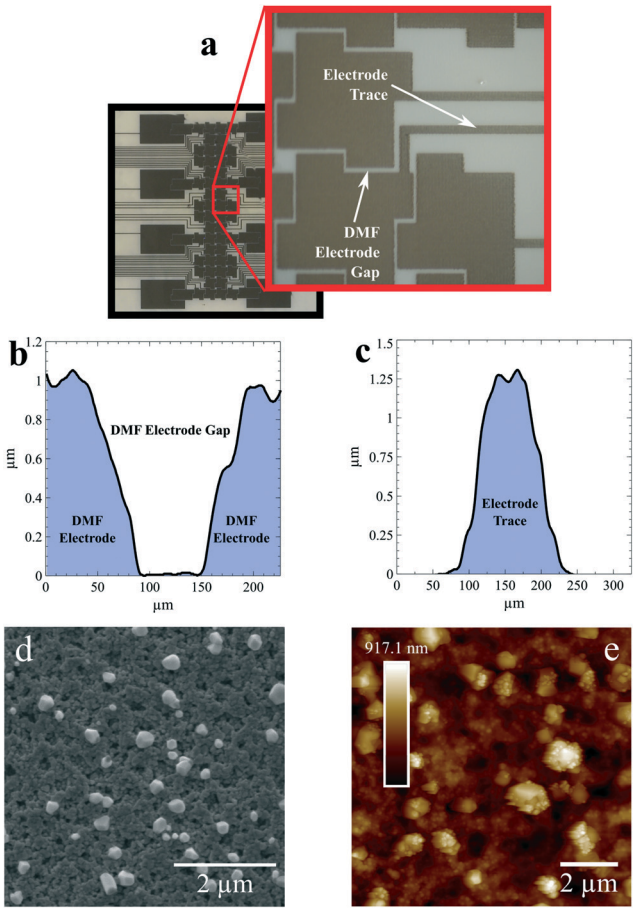

Fig. 2 IJP DMF electrode characterization. (a) Photograph of IJP bottom plate with magnified inset. Contact profilometry data for (b) the gap between two adjacent electrodes, and (c) a cross-section of an electrode trace. (d) Scanning electron microscopy (SEM) micrograph of printed electrode. (e) Atomic force microscopy (AFM) image of printed electrode. The heat-map on the left indicates height (ranging from dark – 0 nm to light – 917.1 nm). The root-mean-square surface roughness is 121 nm.

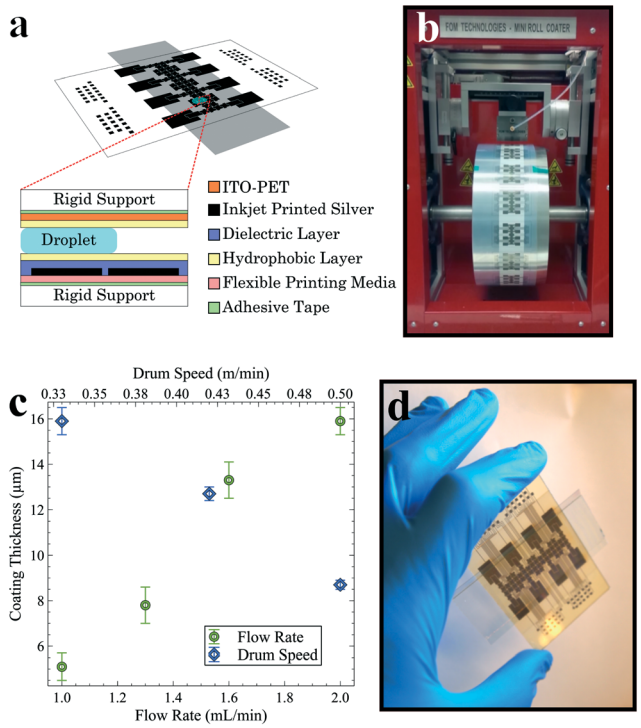

Fig. 3 Roll-coating of DMF devices. (a) Isometric-view schematic indicating how DMF top and bottom plates are mated together. Call-out: cross-section image (not to scale) of a complete two-plate device bearing IJP electrodes (black) coated with dielectric (purple) and hydrophobic (yellow) layers. In practice, devices are usually mounted on rigid substrates (white) with adhesive (green). (b) Photo of a roll of IJP bottom plates loaded onto a FOM Technologies Mini Roll Coater. (c) Thickness of CEP layer measured by contact profilometry as a function of flow rate (green, bottom x-axis, with drum speed set to 0.33 m min^{-1}) and drum speed (blue, top x-axis, with flow rate set to 2.0 mL min^{-1}). Error bars represent ±1 standard deviation. (d) Picture of a fully assembled IJP-RC/RC-DMF device with roll-coated top- and bottom plates.

of IJP electrodes (including the particles) was ~121 nm, a value that is similar to those reported in the literature.[35,41,42]

Roll-coating and device assembly

Armed with a robust, inexpensive method for forming arrays of electrodes, we turned our attention to the (many) other aspects of fabrication and assembly inherent to digital microfluidics. As illustrated in Fig. 3a, two-plate DMF devices are formed from one substrate bearing an array of electrodes (IJP, as above) coated with a dielectric (purple) and a hydrophobic (yellow) coating. Droplets are manipulated by applying electric potentials between driving electrodes on the bottom plate and a counter electrode on a top plate, that is also coated with a hydrophobic material. In the new method introduced here, both plates were formed from flexible materials – Novele (pink) for the bottom plate (as described above), and ITO-coated PET (orange) for the top plate [both finally mounted with tape (green) on rigid substrates (white) prior to use]. Flexible substrates were required for the roll-coating techniques introduced here.

The previous reports[34,35] of IJP DMF devices ignored the steps of dielectric and hydrophobic layer-coating (in practice, both of the previous reports used vapour deposition and spin-coating, techniques that are typically associated with cleanroom fabrication). Here, we addressed this critical limitation by introducing roll-coating (RC) to the digital microfluidic fabrication canon. The particular instrument used here is a slot-die roll-coating system (Mini Roll Coater, FOM Technologies, Lyngby, Denmark), which has been used previously to fabricate organic solar cells in a roll-to-roll format.[43,44] This paper constitutes the first example of applying the technique to fabricate DMF devices.

The RC-DMF process is initiated by affixing a roll of top-plate or bottom-plate substrates onto the roll coater (Fig. 3b). The drum then rotates at a pre-set rate as the solution to be applied is pumped through the slot die head at a pre-set flow rate. In the work reported here, DMF bottom plates were coated first with a dielectric coating formed from Cyanoresin

CR-S cyanoethyl pullulan (CEP), and then again with a hydrophobic coating formed from the amorphous fluoropolymer, FluoroPel PFC 1101V; DMF top plates were coated only with FluoroPel. While the devices described here were formed using a single roll-coater (with interchangeable slot-die heads used for the different coatings), a key advantage of this technique is that it is straightforward to adapt this type of protocol to a larger roll-to-roll (R2R) processing instrument for mass production.[45]

For both types of procedures, the flow rate and drum speed were optimized to yield contiguous, conformal coatings that are free of defects. Fig. 3c illustrates how the CEP coating thickness can be controlled by varying either the drum rotation rate or the flow rate of the coating solution through the slot-die head; the optimum conditions developed for both types of coating are recorded in the methods section. CEP has been previously reported for use as a dielectric in DMF applications[46] and was chosen here for its compatibility with forming thick, defect-free coatings, and for its high relative permittivity of $\varepsilon_r = 19$ (allowing for smooth droplet movement at lower applied voltages[47]). Finally, RC-DMF devices were diced into individual chips, mated to rigid supports with adhesive tape, and assembled to form the completed device as illustrated in Fig. 3d. The final critical materials-cost for a fully assembled two-plate, inkjet printed, roll-coated digital microfluidic (IJP-RC/RC-DMF) device is US $0.63 USD (see the online ESI† for a cost breakdown).

A substantial goal in the work reported here was to develop an inexpensive, scalable method for forming devices, but one that did not sacrifice device performance. As shown in Fig. 4a (and in movie M1 in the online ESI†), devices fabricated using the new methods facilitate robust, smooth droplet movement. The best metric for evaluating DMF device performance is droplet velocity (a function of both the driving forces and the resistive forces that oppose droplet movement[39]), which can be conveniently evaluated using the capacitance feedback of the open-source DropBot control system.[38] The performances of the new and conventional DMF devices were compared, pitting the inkjet printing and roll-coating devices (DMF-IJP-RC/RC) *versus* those formed from conventional photolithography and etching, vapour deposition, and spin-coating (DMF-PLE-VD-SC/SC; note that these devices are the "gold standard" for this field, and were used only for comparison). As shown in Fig. 4b, the absolute velocities and the trend with respect to driving force for devices formed using the new technique (green) are nearly identical to those formed using conventional techniques (blue), particularly at high driving forces. This is a remarkable result given the significant differences between the two kinds of devices (different electrode and coating materials and thicknesses, different rigidities, *etc.*), indicating that devices formed using the new inexpensive, scalable manufacturing techniques reported here do not suffer appreciable drop-off in performance relative to conventional devices formed in the cleanroom.

Finally, we reiterate the ultimate goal of this project, which was to develop an inexpensive device fabrication

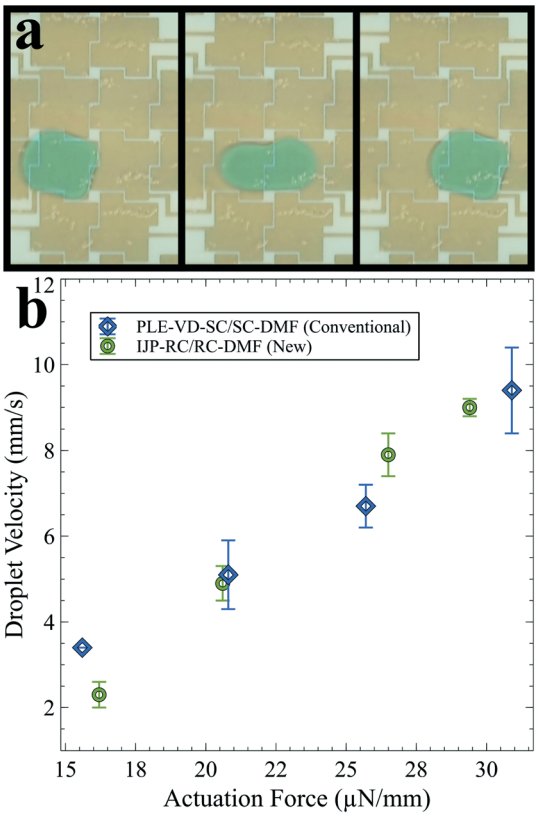

Fig. 4 Droplet movement on inkjet printed, roll-coated DMF (IJP-RC/RC-DMF) devices. (a) Frames from a video (left-to-right) demonstrating movement of a 1.2 μL droplet of wash buffer on an IJP-RC/RC device; the video is found in the online ESI.† Blue dye was added to aid in visualization. (b) Velocities for identical droplets plotted as a function of the driving force for conventional PLE-VD-SC/SC devices (blue) compared to devices formed using the new IJP-RC/RC method (green). Error bars represent ±1 standard deviation for at least 3 droplets evaluated on at least 2 different devices.

method that is directly scalable to mass production. The roll-coating process meets this standard "as is," but we acknowledge that the commercial printer used here does not. To scale this process further, one would need to use an inkjet printing system with in-line sintering that is integrated into a roll-to-roll processing line; there are numerous examples of such systems in the literature.[48,49] But it should be noted that the method described here can also be positioned for accessibility (in place of scalability). For those who are most interested in accessibility, the devices described here can be manually dip-coated with CEP and FluoroPel and operated with similar performance (data not shown) in a process that requires only a ~US $100 printer.

Heterogeneous RV IgG ELISA

Armed with an inexpensive, scalable method for fabricating IJP-RC/RC-DMF devices, we turned to evaluating their performance for implementing a model diagnostic assay for rubella. Rubella virus (RV) is an infectious disease that, while being manageable for healthy adults, poses a significant risk

to pregnant patients, who can pass the disease to their children.[50] Specifically, newborns whose mothers were infected with RV during early pregnancy are at high risk of suffering from congenital rubella syndrome (CRS), a condition associated with intrauterine death and/or debilitating developmental anomalies.[50] As the detection of RV is almost exclusively performed in centralized laboratories,[51,52] there is great need for reliable surveillance in populations where access to such facilities may not be present.[53]

We demonstrated previously that DMF is suitable for the complex operations required for RV detection, with laboratory-quality performance, *i.e.*, 100% clinical sensitivity and specificity for RV IgG and IgM in a panel of serum samples.[36] This previous study relied on conventional, expensive PLE-VD-SC/SC-DMF devices; here, we developed analogous procedures using the new IJP-RC/RC-DMF scheme. Fig. 5a illustrates the 13-step RV assay, which comprises a series of RV-modified-magnetic particle pull-down steps to expose the particles to droplets of sample, wash buffer, antibody-HRP conjugate, enzyme-substrate, and enhancer. Two samples were processed simultaneously with pre-programmed protocols performing the various steps with the entire assay taking approximately 30 minutes to complete. Fig. 5b shows a 4-point calibration curve generated by evaluating a series of rubella virus IgG standards ranging from 0–75 IU mL^{-1} in triplicate. The data was fit by least squares to the four parameter logistic nonlinear regression model, with a LOD of 0.02 IU mL^{-1}, and a LOQ of 0.03 IU mL^{-1}, both well below the diagnostic cut-off of 10 IU mL^{-1} defined by the World Health Organization for RV immunity.[54] To illustrate how the ability to perform complex, multi-step operations is integral to assay performance, we performed the RV ELISA described above while varying the number of washing steps included in the procedure. Fig. 5c demonstrates that as the number of washing steps is increased, the signal-to-background ratio increases dramatically. This emphasizes the importance of the

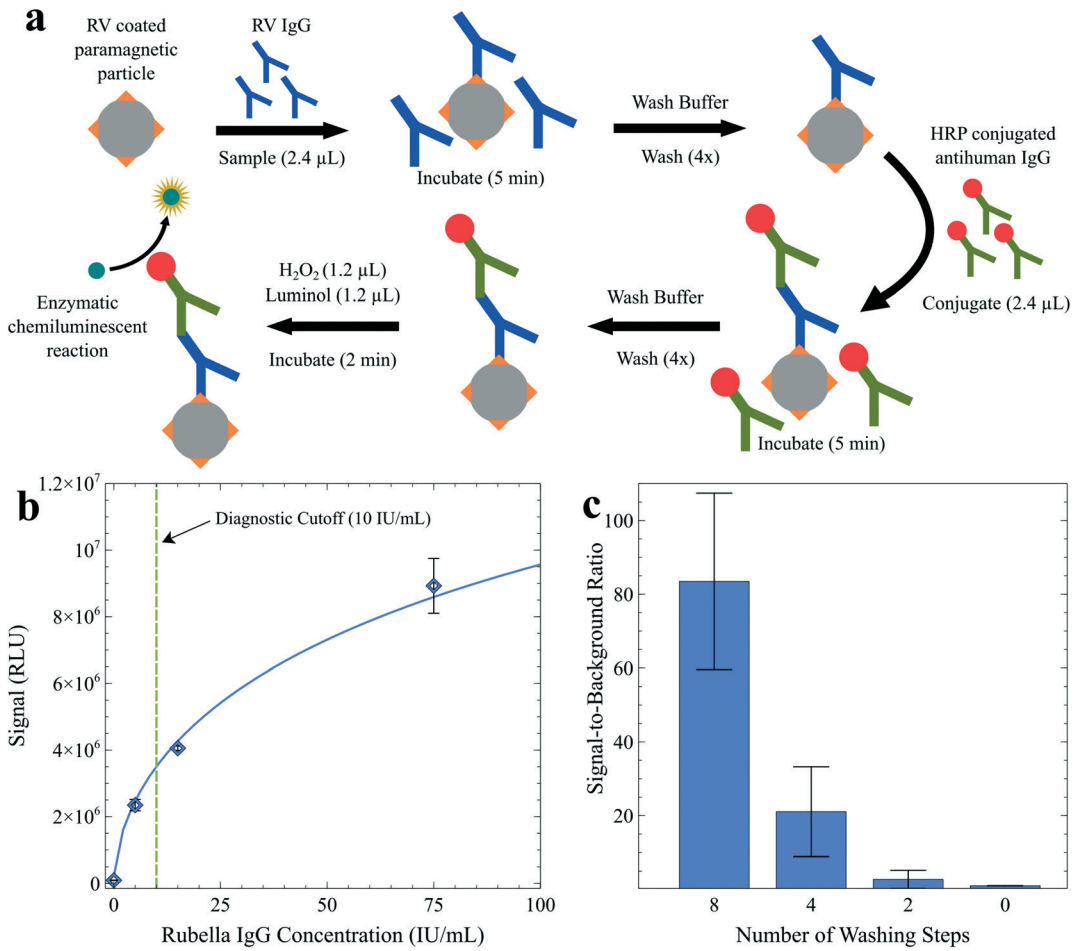

Fig. 5 RV IgG ELISA on IJP-RC/RC-DMF devices. (a) Scheme demonstrating the 13-step assay. Paramagnetic particles (gray) coated with virus (orange) are mixed with sample containing RV IgG antibodies (blue). Successive wash buffer droplets remove unbound RV IgG. The particle-IgG complex is then mixed with HRP conjugated to antihuman IgG (red-green) after which unbound antibody/conjugate is removed in successive wash buffer droplets. H_2O_2 and luminol-enhancer solution droplets are introduced and the chemiluminescence is measured. (b) RV IgG calibration curve for the ELISA implemented on IJP-RC/RC-DMF devices. (c) Investigation into the effect the number of washing steps has on the signal (measured from 5 IU mL^{-1} solution)-to-background (measured from 0 IU mL^{-1} solution) ratio of the ELISA implemented on IJP-RC/RC-DMF devices. Error bars represent ±1 standard deviation.

ability to complete multi-step procedures (with many integrated wash-steps) for performing the RV analysis, tasks not easily accomplished on LFA devices.

Conclusion

We have developed a new method to fabricate two-plate DMF devices. In addition to using an inexpensive, consumer-grade inkjet printer to form the electrodes, for the first time, the application of hydrophobic and dielectric layers was completed with a roll-coating method that is straightforward to scale up to an integrated roll-to-roll method for mass production. Remarkably, these new devices' droplet driving velocities were found to be on par with those formed with traditional cleanroom techniques, with a materials cost for the new devices of less than $1 per device. Devices formed using the new method were demonstrated to be useful for performing complex, multi-step diagnostic assays, leading us to propose that these new devices will serve as an attractive alternative to LFAs without sacrificing assay performance, portability, or cost.

Acknowledgements

We thank Dr. Mohtashim Shamsi (So. Illinois Univ.), Stephen Ho (Univ. of Toronto), and Michael D. M. Dryden (Univ. of Toronto) for fruitful conversations. We thank Prof. Dwight Seferos (Univ. of Toronto) for access to the AFM. We thank the Canadian Foundation of Innovation (CFI), the Ontario Research Fund (ORF), the Natural Sciences and Engineering Research Council of Canada (NSERC), Grand Challenges Canada, and Abbott Diagnostics for funding. M. B. M. is grateful for an Ontario Graduate Scholarship. A. R. W. thanks the Canada Research Chair (CRC) program for a CRC.

References

1 P. Yager, T. Edwards, E. Fu, K. Helton, K. Nelson, M. R. Tam and B. H. Weigl, *Nature*, 2006, **442**(7101), 412–418.
2 A. Kumar, D. Roberts, K. E. Wood, B. Light, J. E. Parrillo, S. Sharma, R. Suppes, D. Feinstein, S. Zanotti, L. Taiberg, D. Gurka, A. Kumar and M. Cheang, *Crit. Care Med.*, 2006, **34**(6), 1589–1596.
3 T. Kabanda, M. J. Siedner, J. D. Klausner, C. Muzoora and D. R. Boulware, *Clin. Infect. Dis.*, 2013, **58**(1), 113–116.
4 S. D. Lawn, A. D. Kerkhoff, M. Vogt and R. Wood, *Lancet Infect. Dis.*, 2012, **12**(3), 201–209.
5 A. W. Martinez, S. T. Phillips, G. M. Whitesides and E. Carrilho, *Anal. Chem.*, 2010, **82**(1), 3–10.
6 X. Li, D. R. Ballerini and Shen W., *Biomicrofluidics*, 2012, **6**(1), 11301.
7 G. E. Fridley, H. Q. Le, E. Fu and Yager P., *Lab Chip*, 2012, **12**(21), 4321.
8 A. W. Martinez, S. T. Phillips, E. Carrilho, W. T. I. Samuel, H. Sindi and G. M. Whitesides, *Anal. Chem.*, 2008, **80**(10), 3699–3707.
9 C. D. Chin, T. Laksanasopin, Y. K. Cheung, D. Steinmiller, V. Linder, H. Parsa, J. Wang, H. Moore, R. Rouse, G. Umviligihozo, E. Karita, L. Mwambarangwe, S. L. Braunstein, J. van de Wijgert, R. Sahabo, J. E. Justman, W. El-Sadr and S. K. Sia, *Nat. Med.*, 2011, **17**(8), 1015–1019.
10 A. W. Martinez, S. T. Phillips and G. M. Whitesides, *Proc. Natl. Acad. Sci. U. S. A.*, 2008, **105**(50), 19606–19611.
11 E. Fu, B. Lutz, P. Kauffman and P. Yager, *Lab Chip*, 2010, **10**(7), 918.
12 X. Li, J. Tian, T. Nguyen and W. Shen, *Anal. Chem.*, 2008, **80**(23), 9131–9134.
13 A. V. Govindarajan, S. Ramachandran, G. D. Vigil, P. Yager and K. F. Böhringer, *Lab Chip*, 2012, **12**(1), 174–181.
14 K. Choi, A. H. C. Ng, R. Fobel and A. R. Wheeler, *Annu. Rev. Anal. Chem.*, 2012, **5**(1), 413–440.
15 K. Choi, A. H. C. Ng, R. Fobel, D. A. Chang-Yen, L. E. Yarnell, E. L. Pearson, C. M. Oleksak, A. T. Fischer, R. P. Luoma, J. M. Robinson, J. Audet and A. R. Wheeler, *Anal. Chem.*, 2013, **85**(20), 9638–9646.
16 A. H. C. Ng, K. Choi, R. P. Luoma, J. M. Robinson and A. R. Wheeler, *Anal. Chem.*, 2012, **84**(20), 8805–8812.
17 J. M. Mudrik, M. D. M. Dryden, N. M. Lafrenière and A. R. Wheeler, *Can. J. Chem.*, 2014, **92**(3), 179–185.
18 M. J. Jebrail, A. H. C. Ng, V. Rai, R. Hili, A. K. Yudin and A. R. Wheeler, *Angew. Chem., Int. Ed.*, 2010, **49**(46), 8625–8629.
19 M. J. Jebrail, N. Assem, J. M. Mudrik, M. D. M. Dryden, K. Lin, A. K. Yudin and A. R. Wheeler, *J. Flow Chem.*, 2012, **2**(3), 103–107.
20 P. Y. Keng, S. Chen, H. Ding, S. Sadeghi, G. J. Shah, A. Dooraghi, M. E. Phelps, N. Satyamurthy, A. F. Chatziioannou, C.-J. C. Kim and R. M. van Dam, *Proc. Natl. Acad. Sci. U. S. A.*, 2012, **109**(3), 690–695.
21 M. R. Javed, S. Chen, J. Lei, J. Collins, M. Sergeev, H.-K. Kim, C.-J. Kim, R. M. van Dam and P. Y. Keng, *Chem. Commun.*, 2014, **50**(10), 1192–1194.
22 V. Srinivasan, *et al.*, *Anal. Chim. Acta*, 2004, **507**(1), 145–150.
23 A. E. Kirby, N. M. Lafrenière, B. Seale, P. I. Hendricks, R. G. Cooks and A. R. Wheeler, *Anal. Chem.*, 2014, **86**(12), 6121–6129.
24 D. G. Rackus, M. D. M. Dryden, J. Lamanna, A. Zaragoza, B. Lam, S. O. Kelley and A. R. Wheeler, *Lab Chip*, 2015, **15**(18), 3776–3784.
25 K.-M. Lei, P.-I. Mak, M.-K. Law and R. P. Martins, *Analyst*, 2015, **140**(15), 5129–5137.
26 S. C. C. Shih, I. Barbulovic-Nad, X. Yang, R. Fobel and A. R. Wheeler, *Biosens. Bioelectron.*, 2013, **42**, 314–320.
27 I. A. Eydelnant, B. Betty Li and A. R. Wheeler, *Nat. Commun.*, 2014, **5**, 3355.
28 A. H. C. Ng, M. Dean Chamberlain, H. Situ, V. Lee and A. R. Wheeler, *Nat. Commun.*, 2015, **6**, 7513.
29 S. Park, P. A. L. Wijethunga, H. Moon and B. Han, *Lab Chip*, 2011, **11**(13), 2212–2221.
30 M. Abdelgawad and A. R. Wheeler, *Microfluid. Nanofluid.*, 2007, **4**(4), 349–355.

31 M. Yafia, S. Shukla and H. Najjaran, *J. Micromech. Microeng.*, 2015, 1–11.
32 M. W. L. Watson, M. Abdelgawad, G. Ye, N. Yonson, J. Trottier and A. R. Wheeler, *Anal. Chem.*, 2006, **78**(22), 7877–7885.
33 A. Abadian and S. Jafarabadi-Ashtiani, *Microfluid. Nanofluid.*, 2014, **16**(5), 989–995.
34 H. Ko, J. Lee, Y. Kim, B. Lee, C.-H. Jung, J.-H. Choi, O.-S. Kwon and K. Shin, *Adv. Mater.*, 2014, **26**(15), 2335–2340.
35 R. Fobel, A. E. Kirby, A. H. C. Ng, R. R. Farnood and A. R. Wheeler, *Adv. Mater.*, 2014, **26**(18), 2838–2843.
36 A. H. C. Ng, M. Lee, K. Choi, A. T. Fischer, J. M. Robinson and A. R. Wheeler, *Clin. Chem.*, 2015, **61**(2), 420–429.
37 R. Liedert, L. K. Amundsen, A. Hokkanen, M. Mäki, A. Aittakorpi, M. Pakanen, J. R. Scherer, R. A. Mathies, M. Kurkinen, S. Uusitalo, L. Hakalahti, T. K. Nevanen, H. Siitari and H. Söderlund, *Lab Chip*, 2012, **12**(2), 333–339.
38 R. Fobel, C. Fobel and A. R. Wheeler, *Appl. Phys. Lett.*, 2013, **102**(19), 193513.
39 R. Fobel, I. Swyer, M. Ho and A. R. Wheeler, 2016, Manuscript in Preparation.
40 J. Stringer, *et al.*, *J. Eur. Ceram. Soc.*, 2009, **29**(5), 913–918.
41 H. C. Jung, S.-H. Cho, J. W. Joung and Y.-S. Oh, *J. Electron. Mater.*, 2007, **36**(9), 1211–1218.
42 D. Kim, S. H. Lee, S. Jeong and J. Moon, *Electrochem. Solid-State Lett.*, 2009, **12**(6), H195.
43 T. R. Andersen, H. F. Dam, M. Hösel, M. Helgesen, J. E. Carlé, T. T. Larsen-Olsen, S. A. Gevorgyan, J. W. Andreasen, J. Adams, N. Li, F. Machui, G. D. Spyropoulos, T. Ameri, N. Lemaître, M. Legros, A. Scheel, D. Gaiser, K. Kreul, S. Berny, O. R. Lozman, S. Nordman, M. Välimäki, M. Vilkman, R. R. Søndergaard, M. Jørgensen, C. J. Brabec and F. C. Krebs, *Energy Environ. Sci.*, 2014, **7**(9), 2925–2933.
44 Y. Lin, H. F. Dam, T. R. Andersen, E. Bundgaard, W. Fu, H. Chen, F. C. Krebs and X. Zhan, *J. Mater. Chem. C*, 2013, **1**(48), 8007–8010.
45 H. F. Dam, T. R. Andersen, M. V. Madsen, T. K. Mortensen, M. F. Pedersen, U. Nielsen and F. C. Krebs, *Sol. Energy Mater. Sol. Cells*, 2015, **140**, 187–192.
46 J. Chen, Y. Yu, K. Zhang, C. Wu, A. Q. Liu and J. Zhou, *Sens. Actuators, B*, 2014, **199**, 183–189.
47 H. Moon, S. K. Cho, R. L. Garrell and C.-J. C. Kim, *J. Appl. Phys.*, 2002, **92**(7), 4080.
48 D. Angmo, T. T. Larsen-Olsen, M. Jørgensen, R. R. Søndergaard and F. C. Krebs, *Adv. Energy Mater.*, 2012, **3**(2), 172–175.
49 J.-S. Yu, I. Kim, J.-S. Kim, J. Jo, T. T. Larsen-Olsen, R. R. Søndergaard, M. Hösel, D. Angmo, M. Jørgensen and F. C. Krebs, *Nanoscale*, 2012, **4**(19), 6032.
50 J. E. Banatvala and D. Brown, *Lancet*, 2004, **363**(9415), 1127–1137.
51 A. M. Bispo de Filippis, J. Icenogle, C. R. Matus and J. K. Andrus, *J. Infect. Dis.*, 2011, **204**(Suppl 2), S652–S658.
52 M. Enders, U. Bartelt, F. Knotek, K. Bunn, S. Strobel, K. Dietz and G. Enders, *Clin. Vaccine Immunol.*, 2013, **20**(3), 420–426.
53 P. A. Rota, K. E. Brown, J. M. Hubschen, C. P. Muller, J. Icenogle, M. H. Chen, B. Bankamp, J. R. Kessler, D. W. Brown, W. J. Bellini and D. Featherstone, *J. Infect. Dis.*, 2011, **204**(Supplement 1), S506–S513.
54 L. P. Skendzel, *Am. J. Clin. Pathol.*, 1996, **106**(2), 170–174.

